Composites Part B 195 (2020) 108075

Contents lists available at ScienceDirect

Composites Part B

journal homepage: www.elsevier.com/locate/compositesb

Nanotailoring of thermoplastic polyurethane by amine functionalized graphene oxide: Effect of different amine modifier on final properties

Madhab Bera, Arjun Prabhakar, Pradip K. Maji *

Department of Polymer and Process Engineering, Indian Institute of Technology Roorkee, Saharanpur Campus, Saharanpur, 247001, U.P., India

ARTICLE INFO

Keywords:
Polyurethane (PU)
Amine functionalized GO (GOA)
Thermo-mechanical properties

ABSTRACT

Thermo-mechanical properties of amine functionalized graphene oxides filled polyurethane (PU) nanocomposites have been investigated in this work. Graphene oxide (GO) was functionalized with *p*-phenylenediamine (PPD), hexamethylene diamine (HMD) and liquid NH_3 separately to check the interaction with the PU matrix. In-situ solution polymerization technique has been adopted for the preparation of nanocomposites. The functionalization of GO with PPD, HMD, and NH_3 was proved by Fourier transform infrared spectroscopy (FTIR), Raman Spectroscopy, X-ray diffraction (XRD), X-ray photoelectron spectroscopy (XPS) and UV–visible spectroscopy. Furthermore, grafting of PU onto the functionalized GO surface has been confirmed from the FTIR and TGA analysis, and the filler dispersion is shown in the respective FESEM and TEM micrographs. With the incorporation of just 0.1 wt% amine functionalized GO, thermal and mechanical properties improve significantly, and the surface becomes more hydrophobic compared to GO filled nanocomposites. Maximum improvement in properties was observed with PPD functionalized GO (GO-PPD) filled PU nanocomposites. At 0.1 wt% loading of GO-PPD, tensile strength, and Young's modulus increases by 378% and 145%, respectively. In addition to these, maximum degradation temperature also increases by 13 °C, which is more than double compared to 0.1 wt% GO filled nanocomposite. Resilience behavior of PU also improves significantly with the addition of amine functionalized GO.

1. Introduction

The segmented polyurethane has several essential properties like high tensile strength, high elongation, tear resistance, excellent abrasion resistance, environmental resistance, chemical resistance, etc. [1]. Its tunable physical properties make it suitable for a wide range of applications like coating, adhesives, foam, composite wood panels, car parts, shoe soles, building insulation, sportswear, insulation material for refrigerators, cushioning of furniture, etc. [1]. However, incorporation of nanofillers into the PU matrix leads to further improvement in physical properties. This is because of the improved interfacial interactions between the highly reactive nanofiller and the PU matrix. Various kinds of nanofiller such as nanoclay [2], carbon black [3], cellulose nanofibers [4], carbon nanotubes (CNTs) [5], graphene [6–8], and modified graphene [9,10] can be used for this purpose. Among the various nanofillers, graphene, and graphene-based materials have drawn significant attention because of their unique combination of properties [11,12]. Functional groups present in the graphene surface play an essential role in the physical properties of the polymer. Hou et al. [13] investigated the effect of amine functionalized graphene on the physicomechanical properties of polyamide 6 (PA6) nanocomposites. The tensile strength of PA6 becomes doubled with the incorporation of 0.1 wt% HMD modified graphene. Pokharel et al. [14] investigated the effect of graphene nanoplatelets, GO, and functionalized graphene sheet (FGS) on the thermo-mechanical properties of polyurethane and found that mechanical properties of 2 wt% GO and FGS filled polyurethane nanocomposites are higher than graphene nanoplatelets filled nanocomposites at similar loading. Ma et al. [15] reported the effect of 3-aminopropyltriethoxysilane (AMEO) functionalized graphene in the properties of polyurethane nanocomposites. With the incorporation of 0.20 wt% functionalized graphene, tensile strength increases by 227%, elongation at break increases by 72%, and thermal stability of polyurethane increases by 50°C compared to pristine polyurethane. Yang et al. [16] investigated the influence of polydopamine functionalized GO in the thermo-mechanical, EMI shielding, UV resistance properties of polydopamine functionalized GO filled polyurethane nanocomposites and found that the fabricated nanocomposite material shows promising results. Nanocomposite film containing 43.3 wt% RGO-HA shows an

* Corresponding author.
E-mail address: pradip@pe.iitr.ac.in (P.K. Maji).

https://doi.org/10.1016/j.compositesb.2020.108075
Received 25 June 2019; Received in revised form 29 March 2020; Accepted 13 April 2020
Available online 20 April 2020

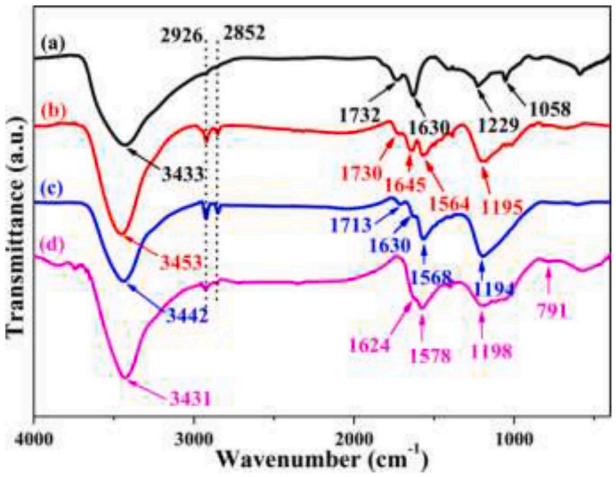

Fig. 1. FTIR spectra of (a) GO, (b) GO-PPD, (c) GO-HMD and (d) GO-NH_3.

82% reduction in the hydrogen gas transmission rate (GTR) compared to a pure nylon film. The effect of hexylamine functionalized reduced graphene oxide (RGO-HA)/polyurethane nanocomposite film in the hydrogen gas barrier property of nylon has been investigated by Bandyopadhyay et al. [17]. Wu et al. [18] investigated the effect of amine functionalized reduced graphene oxide (NH_2-RGO) synthesized by reacting GO with toluene diisocyanate (TDI) and then subsequent reduction by hydrazine, in the thermal and mechanical properties of waterborne polyurethane nanocomposites. With the incorporation of 1.0 wt% NH_2-RGO, tensile strength increases by 73% and storage modulus increases by 973%. Thermal stability also increases by 40°C. There are various other reports available where functionalized graphene has a positive impact in the properties of polyurethane nanocomposites [19,20].

The effect of structural disparity coming from the difference in hydroxyl and carboxyl group contents in GO and RGO on the thermo-mechanical and surface properties of PU has been discussed in our previous work [21] where filler content was varied from 0.05 to 0.20 wt % and found a remarkable improvement in thermal and mechanical properties of PU nanocomposites at ultra-low loading (0.1 wt%). So, the current study will be the effect of amine functionalized GO (GOA) on the properties of thermoplastic polyurethane at ultra-low loading. The reason behind the selection of amine functionalized GO as reinforcing material is the easy dispersibility of small chain primary amine functionalized GO in the organic compound and better interaction with the polymer matrix [13]. After a thorough literature survey, it is found that there are various discrete reports on the effect of graphene, GO, RGO, and functionalized graphene on the thermal, mechanical properties of polymer nanocomposites. However, there is no such report which clearly explains the effect of different types of amine functionalized GO on thermo-mechanical and surface properties of TPU nanocomposites. Since strong interfacial interaction between the polymer and filler leads to improvement in thermal, mechanical, and other properties, the aim of this work is to improve the interfacial interaction between TPU and GO by amine functionalization of GO. For this purpose, GO has been modified with various amine modifiers like *p*-phenylenediamine (PPD), hexamethylene diamine (HMD) and liquid NH_3 and the effect of these modifications in morphologies, thermal, mechanical and surface properties of PU nanocomposites has been investigated in this work.

2. Experimental

2.1. Materials

Graphite flakes (~150 μm), PTMEG (M_n=2000), 4,4′-MDI, hexamethylene diamine (HMD), thionyl chloride (97%), and *p*-phenylenediamine (PPD) were purchased from Sigma-Aldrich, Germany. 1, 4 butanediol, dimethylformamide (DMF), dibutyltin dilaurate (DBTL), diethyl ether, hydrochloric acid (HCl), sulfuric acid (H_2SO_4), were obtained from Hi-Media Laboratories Pvt. Ltd., India. Liquid ammonia (25% assay) was purchased from Sisco Research Laboratories Pvt. Ltd. (SRL), India. Hydrogen peroxide (30% assay), potassium permanganate ($KMnO_4$) and phosphoric acid (H_3PO_4) were purchased from Rankem India. PTMEG was dried in a vacuum oven at 65 °C for 24 h. Both DMF and butanediol were dried by using 4 Å molecular sieves. The rest of the chemicals were used as obtained.

2.2. Synthesis of graphene oxide (GO)

GO was synthesized by oxidation of graphite flakes with $KMnO_4$ in 9:1(v/v) mixture of H_2SO_4 and H_3PO_4, followed by washing and purification using centrifugation as described in our previous report [22]. The synthesis of GO was confirmed by XRD, FTIR, and XPS, and the formation of monolayer GO sheets was confirmed by using AFM and TEM analysis.

2.3. Synthesis of p-phenylenediamine functionalized GO (GO-PPD)

200 mg GO was dispersed in 200 ml distilled water by ultrasonication for 2 h in a bath sonicator (100 W). 2 g PPD was dissolved in 100 ml of distilled water at 70 °C for 1 h and added to the GO dispersion. Subsequently, a 1.2 ml NH_3 solution (25% w/v) was added, and the reaction was continued for 6 h at 95 °C temperature. After the completion of the reaction, the product was filtered through a 0.2 μm membrane filter. The residue was dispersed in ethanol, ultrasonicated for 5 min, and then filtered through the membrane filter. The process of dispersion, sonication, and filtration was carried out 5–6 times to remove the unreacted and excess PPD. The product was dried in an oven of at 50 °C for 24 h [23]. The resulting material was designated as GO-PPD.

2.4. Synthesis of hexamethylenediamine functionalized GO (GO-HMD)

300 mg GO was dispersed in 300 ml of anhydrous DMF (1 mg/ml) by overnight stirring, followed by 2 h bath sonication. 30 ml $SOCl_2$ was added to the GO dispersion at 1:10 vol ratio of $SOCl_2$ and GO dispersion, and the reaction mixture was heated at 70 °C temperature for 2 h. It was then allowed to cool down to room temperature and centrifuge to obtain the GO-Cl slurry. The solid residue was re-dispersed in dry DMF and centrifuge again. This process was repeated thrice to remove the excess and unreacted $SOCl_2$. The final residue was coagulated in 50 ml dichloromethane (DCM) and filtered through a 0.2-μm nylon filter. The residue was washed with 50 ml DCM and then dried in a 50 °C oven for 24 h [24].

300 mg GO-Cl was dispersed in 300 ml ethanol by ultrasonication. 1.2 g HMD was added to the GO-Cl dispersion, and the reaction was continued for 2 h at 60 °C in a bath sonicator. The reaction mixture was cooling down to room temperature and filtered through a 0.2-μm membrane filter. The remaining solid material was washed with ethanol several times to remove unreacted HMD, dried at 50 °C temperature for 24 h [25]. The resulting material was designated as GO-HMD.

2.5. Synthesis of ammonia functionalized GO (GO-NH_3)

300 mg GO was dispersed in 120 ml ethylene glycol by overnight stirring and 2 h sonication in a bath sonicator (100 W) to get a brown colored homogeneous dispersion. 3 ml liquid ammonia solution (25% in water) was added to the dispersion, and the resulting mixture was refluxed in a round-bottomed flux fitted with a water-cooled condenser at 180 °C for 12 h. After 12 h, the reaction mixture was allowed to cool down to room temperature and vacuum filtered through a 0.2-μm nylon filter.

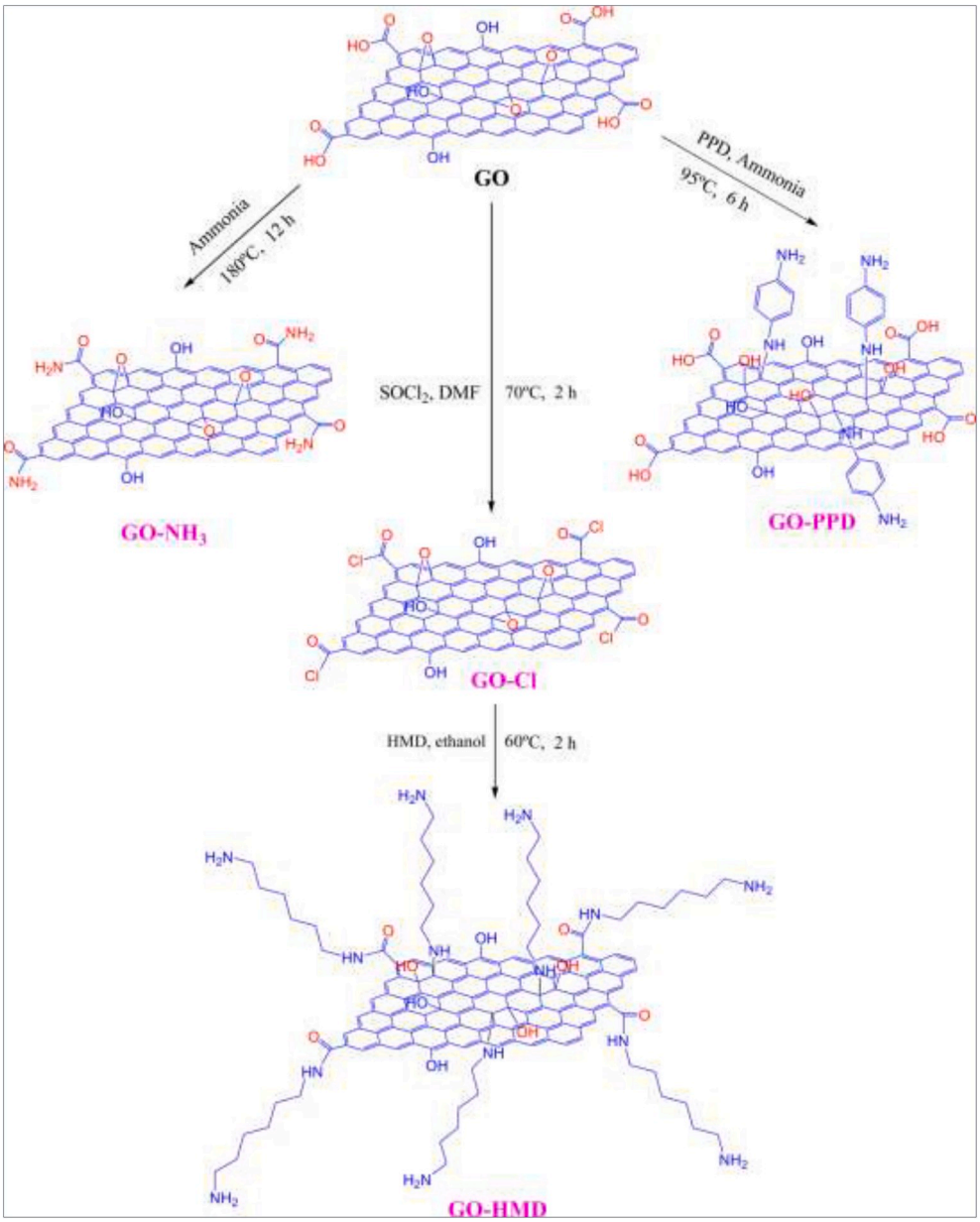

Fig. 2. Amine functionalization of GO using PPD, HMD, and NH_3.

The black-colored solid residue was repeatedly washed with distilled water until the pH of the filtrate was neutral, checked by pH paper. The final material was dried in a 50 °C oven. The prepared material was designated as GO-NH_3 and used for further characterization and use [26].

2.6. In-situ synthesis of TPU/amine functionalized GO nanocomposites

TPU nanocomposites were fabricated by in-situ polymerization technique. 10 g (5 mmol) PTMEG was taken in a 250 ml three necks round bottom flask fitted with a water-cooled condenser. 10 ml dried DMF was added to it, and the materials were heated up to 65 °C under the nitrogen atmosphere. A stoichiometric excess of MDI (3 g, 12 mmol) was dissolved in 10 ml DMF and injected into the reaction mixture by using a syringe. The reaction temperature was maintained at 65 °C for 2 h, under constant stirring, to produce isocyanate-terminated polyurethane prepolymer. The required amount of GO and amine-modified GO was dispersed in 10 ml dried DMF with the help of ultrasonication and added to the polyurethane pre-polymer. The reaction temperature was cooling down to 40 °C.

During this time, amine functionalized GO react with the isocyanate-terminated polyurethane prepolymer and the prepolymer attached to the modified GO surface. 0.45 g (5 mmol) 1,4-butanediol and two drops DBTL were injected into the medium after dissolving 5 ml DMF in each case. The reaction temperature was slowly raised to 75 °C. Temperature and stirring was maintained for another 4 h. The increase in viscosity of the medium indicates the formation of polyurethane nanocomposites. The solid content of the synthesized material was adjusted to ~20%. The materials were cast into a Petri dish and keep it into a 50 °C hot air oven for three days to remove the solvent slowly. The residual amount of DMF was removed by placing the film in a 90 °C vacuum oven for one day. The synthesized polyurethane nanocomposites were designated as TPU/GO 0.1, TPU/GO-PPD 0.1, TPU/GO-HMD 0.1, TPU/GO-NH_3 0.1 according to the nanomaterials added [21].

3. Characterization

Wide-angle powder XRD (Rigaku Ultima IV, Japan) was used for the

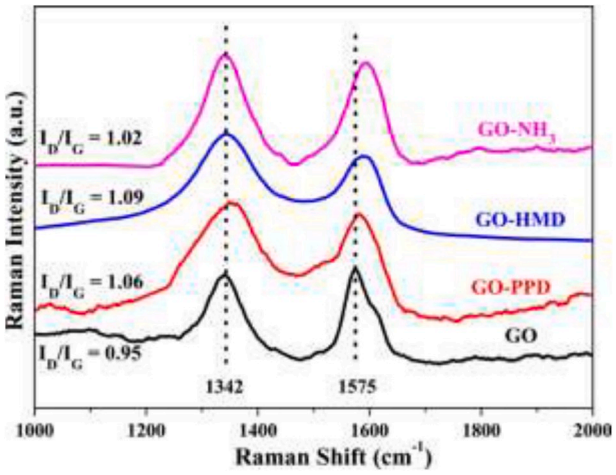

Fig. 3. Raman spectra of GO, GO-PPD, GO-HMD and GO-NH_3.

structural characterization of GO, GO-NH_3, GO-HMD, and GO-PPD. The standard operating conditions were $\lambda_{CuK\alpha}$ = 1.54 Å, scan range was between 5° to 60°, and the scan rate was 4 °C/min. Results are shown in supporting information.

FTIR spectra of GO, GO-NH_3, GO-HMD, and GO-PPD were recorded in PerkinElmer Spectrum Two FTIR instrument with KBr pellets. FTIR spectra of polyurethane and its nanocomposite films were recorded in attenuated total reflectance (ATR) mode. In all cases, the samples were scanned at a scan rate of 4 cm^{-1} and an average 16 scan per sample.

FT-Raman Spectrophotometer (BRUKER RFS 27: Standalone model) was used for the Raman spectroscopy analysis of GO and amine functionalized GO within the scan range 1000–2000 cm^{-1} at a scan rate of 2 cm^{-1}. The laser source is Nd: YAG with a wavelength of laser light λ = 1064 nm.

Elemental analysis of all nanomaterials was performed by using X-ray Photoelectron Spectroscopy (XPS) (Physical Electronics, PHI 5000 Versa Probe III, USA). For TPU and its composites, the polymer-filler interaction was investigated by using X-ray Photoelectron Spectroscopy (XPS) (Omicron nanotechnology, Oxford Instrument, Germany). Aluminium Kα (energy = 1486.7eV) was used as a monochromatic X-ray source. The instrument was operated at 15 kV and 20 mA, and the pass energy for the high-resolution scan was 20eV.

UV-VIS spectroscopy of all nanomaterials was performed in a Shimadzu UV 1800 instrument within the wavelength range of 200–700 nm. The concentration of samples was 0.05 mg/ml in water. UV–Vis spectra of GO and amine functionalized GOs are shown in Supporting Information.

Universal Testing Machine (Model No 3365, Instron Co., Macclesfield, UK) was used to measure the tensile properties of the samples. Testing was done as per ASTM D 412, at a crosshead speed of 100 mm/min by using a 5 kN load cell. The average result of five measurements for each sample was reported. The cyclic tensile test was also performed in the same UTM instrument at 200% elongation, 100 mm/min speed, and up to 10 cycles to check the resilience value.

EXSTAR TG/DTA 6300 (SII NanoTechnology Inc.) instrument was used for thermogravimetric analysis (TGA) of all the samples. Testing was carried out under a nitrogen atmosphere at a heating rate of 10 °C min^{-1} from room temperature to 800 °C. TGA of GO and amine functionalized GOs are shown in Supporting Information.

Morphological characterization was done by field emission scanning electron microscopy (MIRA3 TESCAN, USA) at a voltage of 10 kV.

Transmission electron microscopy (TEM, Tecnai G2 20S–TWIN, FEI Netherlands) was used for morphological characterization of GO, RGO, amine functionalized GO, and their polymer nanocomposites. The nanomaterials were dispersed in a suitable solvent at 0.01 mg/ml concentration and ultrasonicated for uniform dispersion. It was kept for few minutes for settling the large particles then drop cast onto a carbon-coated Cu grid of 400 mesh sizes. The composite samples for TEM were prepared by cryo-ultramicrotomy with a Leica Ultracut UCT (Leica Microsystems GmbH, Vienna, Austria). Freshly sharpened glass knives with cutting edge of 45° were used to obtain cryosections of 120 nm thickness at −90 °C temperature. The samples were then transferred to 400 mesh carbon-coated Cu TEM grids. Images were taken with a transmission electron microscope (TEM, Tecnai G2 20S–TWIN, FEI Netherlands). Bright-field TEM images of all samples were recorded.

Surface polarity, work of adhesion, and surface energy were determined by contact angle measurement (Phoenix 300, Korea). The measurement was done by the sessile drop method by placing a drop of water having volume 6 μl on the sample surface. In the case of GO, RGO and amine functionalized GO, and a clean glass surface was coated with the nanodispersions and dried to form a uniform layer of the nanomaterials on the glass surface. The coated glass surface was used for contact angle analysis.

The dynamic mechanical property of neat TPU and its nanocomposite films were analyzed by Anton Paar Rheometer, MCR-102 in DMTA tension mode at a constant frequency of 1 Hz. The rectangular sample used in this testing was approximately 40 mm × 5 mm x 0.50 mm in dimensions. All the samples were first cooled to −100 °C by using liquid nitrogen and then scanned within the temperature range −100 °C to 60 °C at a heating rate of 5 °C/min.

4. Results and discussion

4.1. Structural characterizations of amine-functionalized GO

4.1.1. Fourier transform infrared spectroscopy (FTIR)

Functional groups present in GO and amine functionalized GO analyzed by FTIR spectroscopy. FTIR spectra of GO, GO-PPD, GO-HMD, GO-NH_3 are presented in Fig. 1. In the case of GO, the bands at 3433 and 1732 cm^{-1} corresponds to the stretching vibration of O–H and C═O, respectively [27]. This observation indicates the presence of hydroxyl, carboxyl, and carbonyl groups within the GO structure. Symmetric and asymmetric stretching of C–H was recorded at 2852 and 2926 cm^{-1}, respectively. The bands at 1630, 1229, and 1058 cm^{-1} correspond to the C═C stretching of aromatic ring, C–O stretching of an alkoxy group, and C–O–C stretching of epoxy groups, respectively [28,29]. This observation confirms the presence of the epoxy group in the GO structure. A similar observation has been reported by many other researchers, also [30]. The FTIR spectra of amine functionalized graphene oxides contain a relatively sharp band within 3430–3460 cm^{-1} corresponding to the N–H stretching vibration of amine and amides [30,31]. The appearance of new bands at 1645, 1564, and 1195 cm^{-1} in GO-PPD was due to C═O stretching of the amide group (–NHCO–), N–H bending, and C–N stretching respectively [31,32]. This observation clearly confirmed the formation of covalent bonding between the COOH or epoxy group of GO and the NH_2 group of the amine modifiers via an SN^2 reaction. Similar results were found in the case of GO-HMD [30] and GO-NH_3 [13] also. In GO-HMD, new bands at 1568 cm^{-1} (N–H bending) and 1194 cm^{-1} (C–N stretching) were observed, confirming the formation of an amide linkage. In this case, the amino group not only reacts with thionyl chloride activated –COOH groups but also reacts with the highly reactive epoxy groups of GO. Further, the appearance of two intense peaks at around 2852 cm^{-1} (symmetric –C-H stretching) and 2926 cm^{-1} (asymmetric –CH stretching) confirms the attachment of HMD to the GO surface (Fig. 2c). For GO-NH_3, new peaks observed at 1578 cm^{-1} (N–H bending) and 1198 cm^{-1} (C–N stretching) due to the formation of an amide linkage. A similar type of FTIR spectra for amine-modified graphene oxide has been reported elsewhere [30,31]. Amine functionalization of GO has been shown schematically in Fig. 2.

4.1.2. Raman Spectroscopy analysis

Functionalization of GO by different types of amine modifiers can be

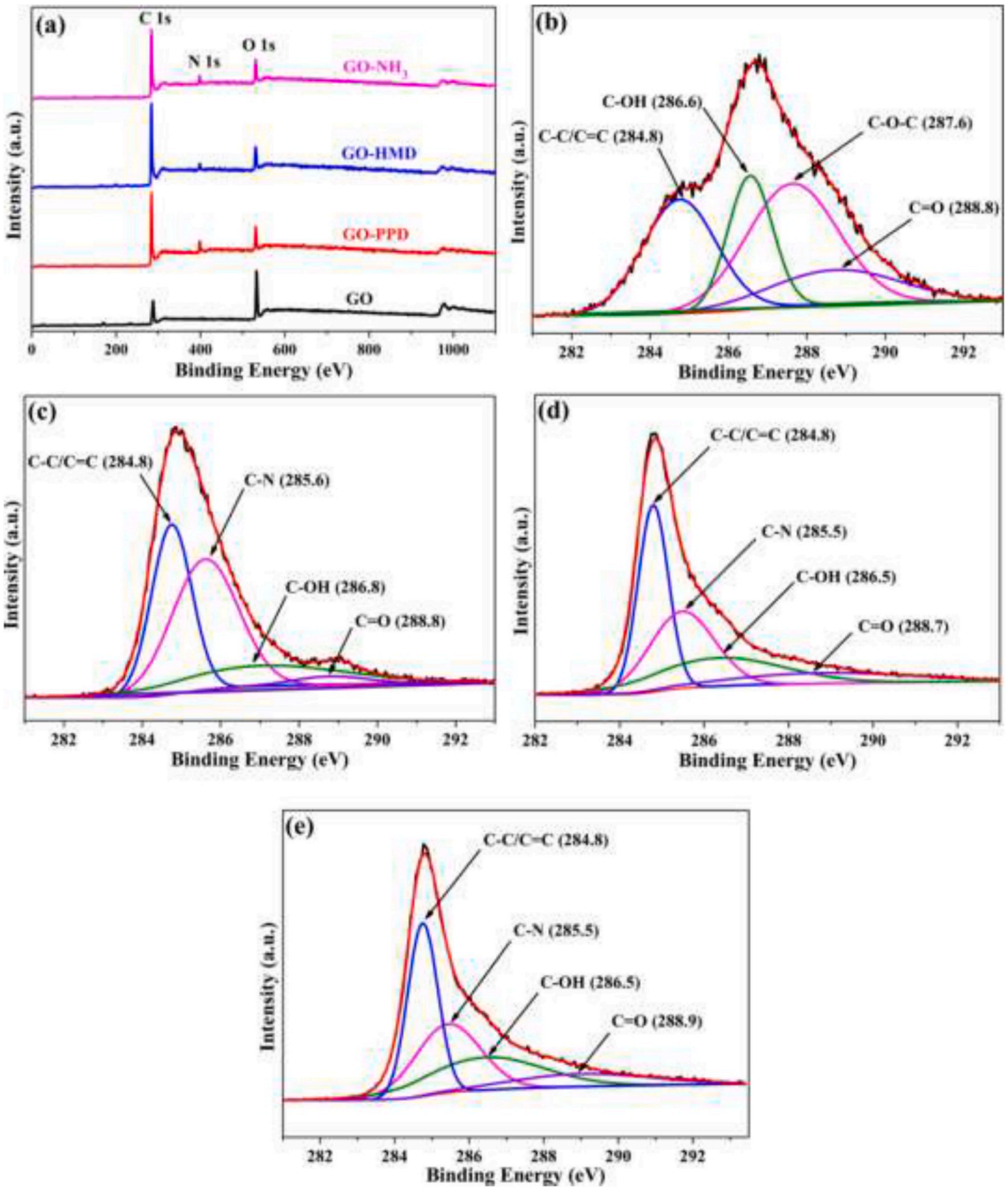

Fig. 4. (a) XPS survey spectra of GO, GO-PPD, GO-HMD and GO-NH_3 (b, c, d, e) C 1s XPS spectra of GO, GO-PPD, GO-HMD and GO-NH_3 respectively.

Table 1
Atomic concentration of GO, GO-PPD, GO-HMD and GO-NH_3 obtained from XPS survey plots.

Sample	Atomic concentration (%)			C/O
	C	N	O	
GO	59.41	0	40.59	1.46
GO-PPD	76.75	10.13	13.12	5.85
GO-HMD	83.11	4.17	12.72	6.53
GO-NH_3	76.92	7.58	15.50	4.96

proved from the Raman spectroscopy of the respective material. As shown in Fig. 3, the Raman spectrum of GO shows to peaks located at 1342 cm^{-1} for D band and 1575 cm^{-1} for the G band. The D band arises due to different types of structural defects or disorder, and the G band arises due to first-order scattering of the E_{2g} phonon of sp2 carbon atoms [17]. The ratio of I_D/I_G increased from 0.95 for GO to 1.06 for GO-PPD, 1.09 for GO-HMD, and 1.02 for GO-NH_3. This implies the removal of oxygen-containing functional groups, the transformation of sp3 carbon of GO into sp2 carbon of amine functionalized GO, and incorporation of structural defects or disorder during functionalization [17,33]. The increase in intensity of D band compared to G band in all amine functionalized GO and increase in I_D/I_G ratio clearly supports the amine functionalization of GO [31].

4.1.3. X-ray photoelectron spectroscopy (XPS)

XPS was employed to determine the surface chemical composition and formation of new chemical bonds during chemical functionalization

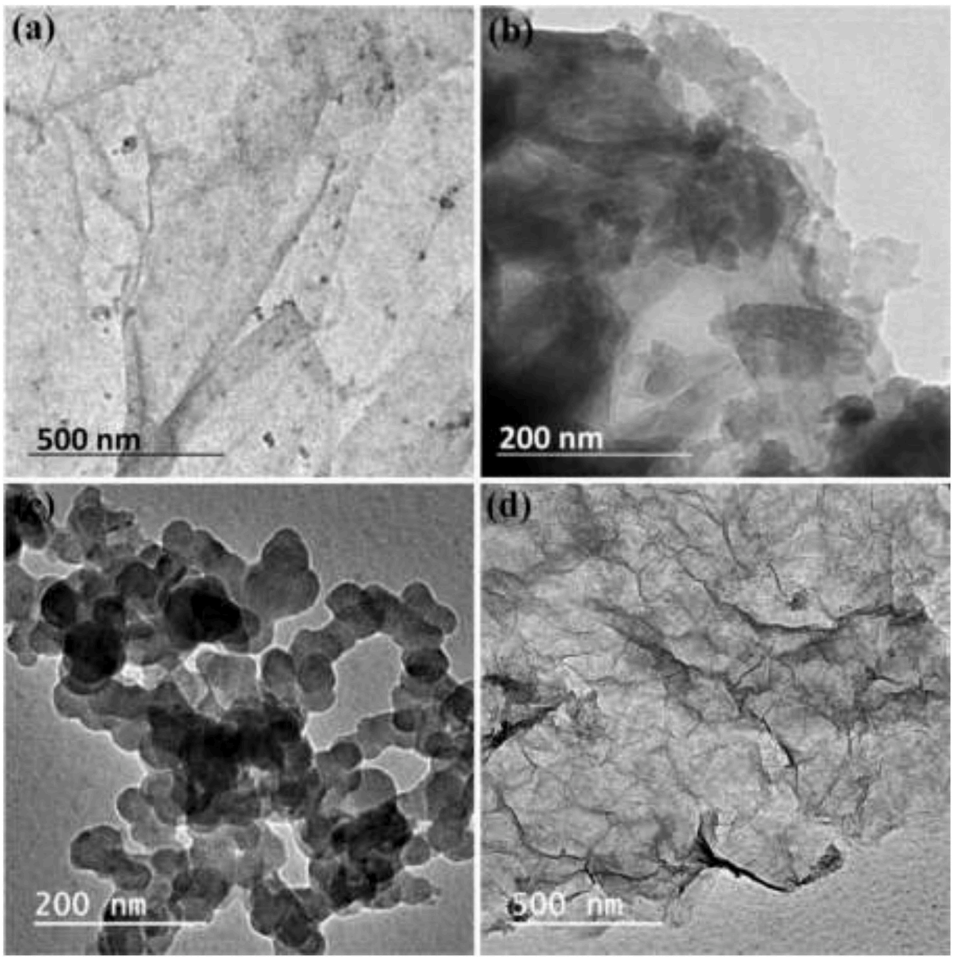

Fig. 5. Bright field TEM images of (a) GO (b) GO-PPD (c) GO-HMD (d) GO-NH_3.

of GO (Fig. 4). As seen in the XPS survey plot (Fig. 4a), all amine functionalized GO contains a new peak for N 1s which was absent in GO. This observation clearly indicate the successful functionalization of GO with PPD, HMD and NH_3. Amount of nitrogen is maximum in GO-PPD (10.13%) and minimum in GO-HMD (4.17%). It was clear that carbon to oxygen atomic ratio (C/O) increases upon amine functionalization. The C/O ratio for GO was 1.46, which increased to 5.85 for GO-PPD, 6.53 for GO-HMD, and 4.96 for GO-NH_3 (Table 1). The observed results confirmed the removal of oxygen-containing functional groups or the reduction of GO during functionalization [34]. Four different peaks were observed in the C 1s spectrum of GO after deconvolution. The peaks emerging at 284.8, 286.6, 287.6, and 288.8 eV corresponds to C–C/C═C in graphite skeleton, C–OH, C–O–C, and C═O, respectively [35]. After the reaction with amines, the peak for the epoxy group disappeared, and a new peak corresponding to the C–N appeared at 285.5 eV in all functionalized GO.

This indicates the successful functionalization of GO via SN^2 reaction between the epoxy groups of GO and the NH_2 groups of amines [11]. The intensity of carbonyl (C═O) and hydroxyl groups (O–H) decreases in all amine functionalized GO compared to pristine GO, signifying the reduction of GO due to amine functionalization. Yuan et al. [35] and Caliman et al. [34] reported a similar type of results.

4.2. Morphological characterization of amine functionalized GO (GOA)

4.2.1. Transmission electron microscopy (TEM)

Morphological characterization has been done by using transmission electron microscopy (TEM). Bright-field TEM image of GO, GO-PPD, GO-HMD, and GO-NH_3 has been shown in Fig. 5.

The bright part of the images indicates less or no stacking of nanosheets, and the dark portion of the image suggests the stacking of several layers [36]. The TEM image of GO shows crumpled and folded morphology, which is due to the existence of oxygen-containing functional groups on GO surface [35]. The folding and crumpling in the nanosheets increase after amine functionalization and become maximum in the case of liquid ammonia functionalized GO (Fig. 5d). This is because of the greater extent of H-bonding between the amine molecules. This type of TEM morphology has been observed by Caliman et al. [34] for *p*-phenylenediamine (PPD), diisopropylamine (DPA), dibenzyl amine (DBA) and piperidine (PA) functionalized GO. By comparing the TEM images, it can be concluded that the layered structure of GO retained ever after amine functionalization.

Structural characterization by XRD, UV-VIS spectroscopy and thermogravimetric analysis of GO and amine functionalized GOs were discussed in the Supporting Information.

4.3. Structural characterization of TPU/amine functionalized GO nanocomposites

Polyurethane contains hard and soft segments within the structure. Crystallization of the segments and phase separation between them play an essential role in determining the properties of polyurethane [37]. Nanofillers have a positive influence in the inter-domain phase separation by acting as a barrier between the hard and soft segment of polyurethane [38]. The grafting of polyurethane chain into the GO and amine functionalized GO surface during the nanocomposite synthesis is

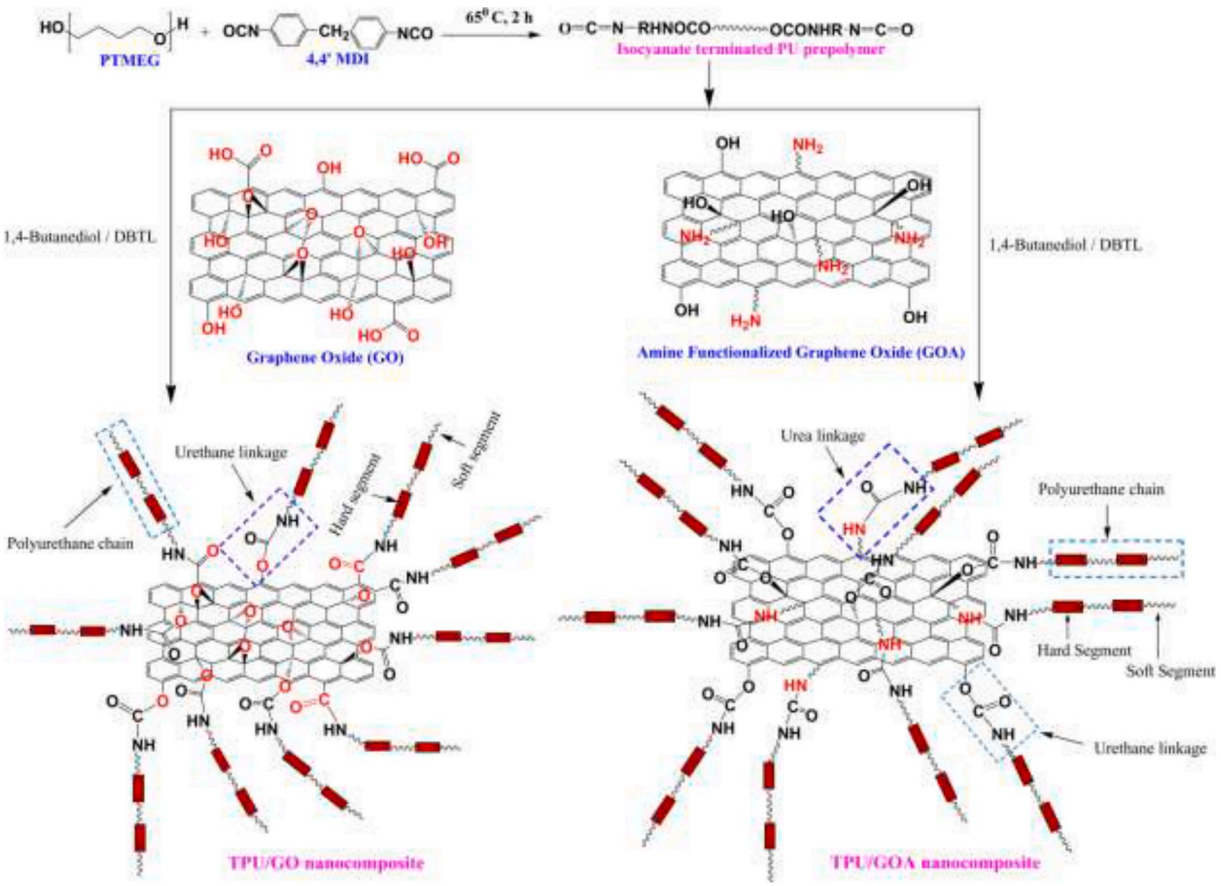

Fig. 6. In-situ functionalization of GO and GOA by TPU and formation of nanocomposites.

shown in Fig. 6. From Fig. 6, it is clear that in case of GO functionalization only urethane linkage is formed between the GO and TPU. But, in case of GOA, urethane as well as urea linkage is formed between the GOA and TPU. FTIR is employed to investigate the interaction between the polyurethane and the nanomaterials and also the H-bonding interaction between the hard segments of polyurethane. Since, N–H and C═O groups of polyurethane only participate in H-bonding, so the changes in the FTIR spectra of nanocomposites will be observed for the said functional groups only. FTIR spectra of TPU and its nanocomposites are presented in Fig. 7. The peak at 3313, 1727, and 1706 cm^{-1}correspond to the H-bonded N–H stretching, free C═O stretching, and H-bonded C═O stretching of TPU, respectively. The characteristic peaks identified for TPU are C–N stretching (1537 cm^{-1}), alkoxy C–O stretching (1221 cm^{-1}), epoxy O–C–O stretching (1104 cm^{-1}), symmetric CH_2 stretching (2854 cm^{-1}) and asymmetric CH_2 stretching (2941 cm^{-1}). In all TPU nanocomposites, the said peaks were observed clearly. This confirms the formation of TPU and its nanocomposites [39]. The absence of a peak at 2270 cm^{-1} confirms that all isocyanates were reacted completely [9]. As the amount of filler added is very low (0.10 wt%), it is quite difficult to get any strong evidence of any kind of interactions from FTIR spectra [8,40]. Only very minor changes in N–H and C═O stretching vibration has been noted (Fig. 7b and c). In all nanocomposites, the intensity of the H-bonded carbonyl group was lower than that of pristine TPU. This observation indicates some interaction between the carbonyl group of TPU and the N–H and O–H groups of amine functionalized GO. Minimal shifting of the N–H peak was also noticed (Fig. 7b). All these observations indicate a significant interaction between TPU and amine functionalized graphene oxide (GOA). Pokharel et al. [9] reported similar results for GO reinforced TPU nanocomposites.

4.4. Morphological characterization of TPU/amine functionalized GO nanocomposites

Dispersion of nanofiller into the polymer matrix and the polymer-filler interaction play an important role in determining the performance of a composite material. Morphological characterization is a direct way to visualize the filler dispersion within the polymer matrix. Here, dispersion of GO, GO-PPD, GO-HMD, and GO-NH_3 within TPU was analyzed by FESEM and TEM analysis. The dispersed fillers within the TPU matrix are pointed by the arrow mark.

4.4.1. Field emission scanning electron microscopy (FESEM) analysis

Fig. 8 represents the FESEM images of the tensile fractured surface of TPU and its nanocomposites with 0.10 wt% of GO, GO-PPD, GO-HMD, and GO-NH_3. The FESEM image of the tensile fractured surface of TPU (Fig. 8a) shows a flat and smooth surface, whereas the same for all nanocomposites are irregular and relatively rough. This is due to the presence of GO and amine functionalized GO.

From Fig. 8, it is clear that all amine functionalized GO is more uniformly distributed within the TPU matrix and exhibits better interaction with TPU compared to GO. This is due to the formation of urea linkage (–NH–CO–NH–) by the reaction of the NH_2 group of amine functionalized GO with the –NCO group of the isocyanate-terminated polyurethane pre-polymer [41]. Fig. 8c shows that the GO-PPD nanosheets are more uniformly distributed than GO-HMD and GO-NH_3. So, GO-PPD will interact better with TPU and hence influences more in the enhancement of physical properties of TPU compared to other amine functionalized GO. This type of morphology has been observed by various researchers [42,43].

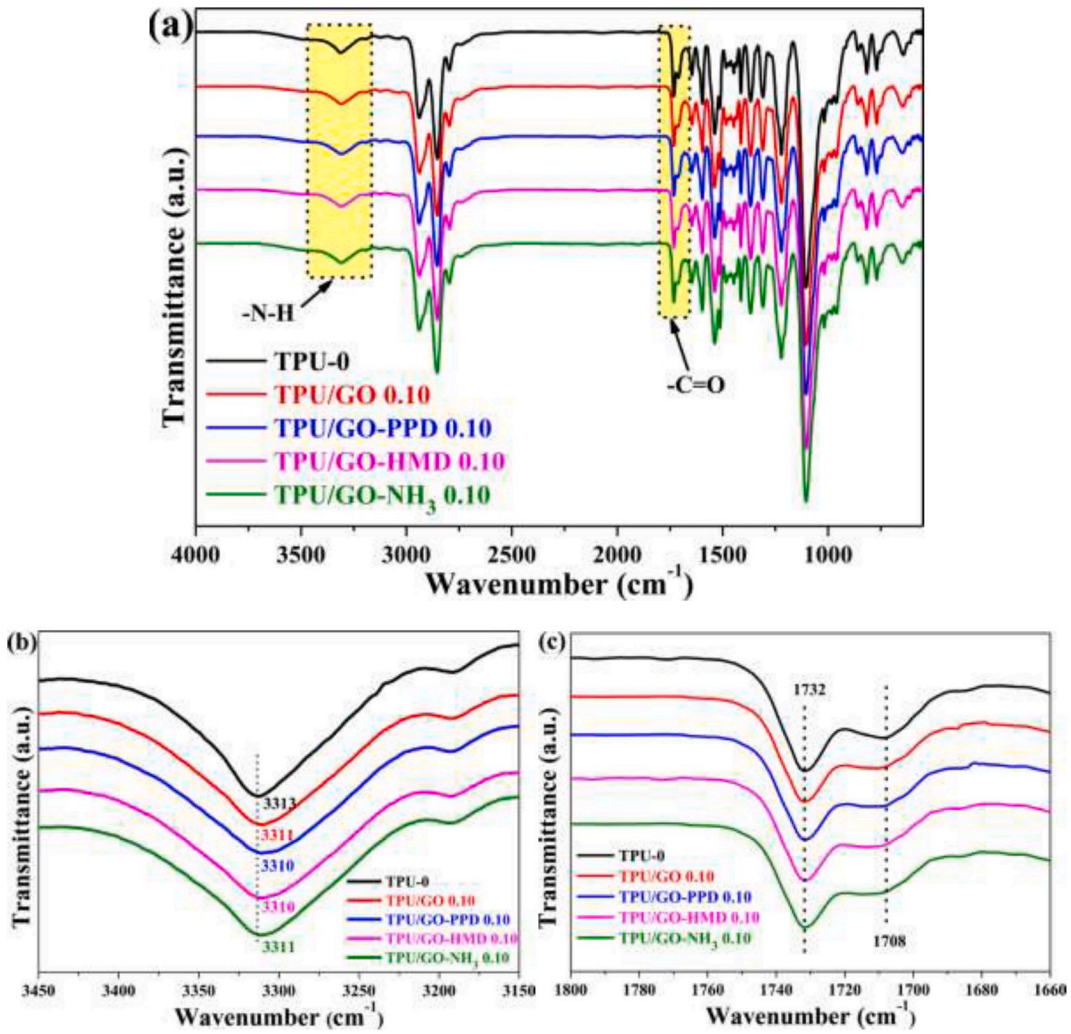

Fig. 7. FTIR-ATR spectra of TPU and its nanocomposites with 0.10 wt% of GO, GO-PPD, GO-HMD, and GO-NH_3 within (a) 4000-550 cm^{-1} (b) 2450-3150 cm^{-1} and (c) 1800-1660 cm^{-1}.

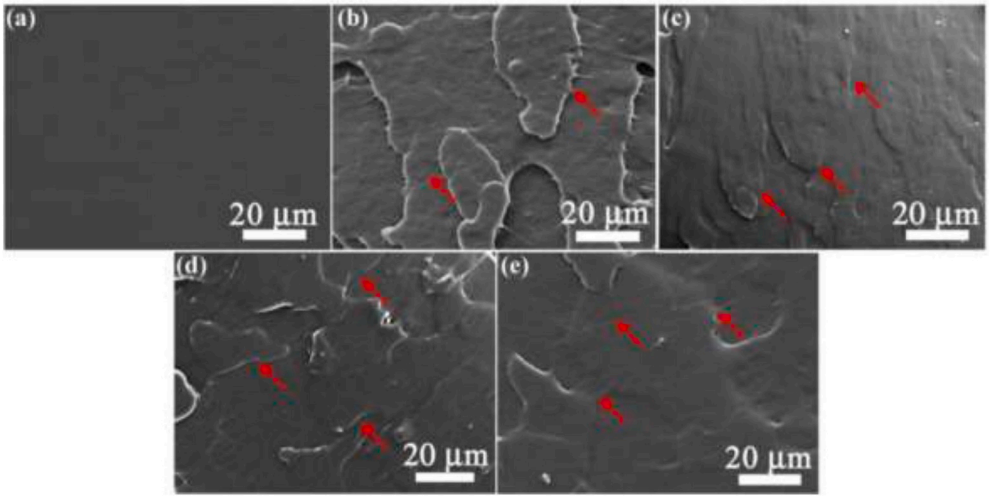

Fig. 8. FESEM image of tensile fractured surface of (a) TPU-0; (b) TPU/GO 0.10; (c) TPU/GO-PPD 0.10; and (d) TPU/GO-HMD 0.10; (e) TPU/GO-NH_3 0.10 samples.

4.4.2. Transmission electron microscopy (TEM) analysis

Transmission electron microscopy (TEM) was employed for direct morphological observation. Bright-field TEM images of TPU/GO 0.10, TPU/GO-PPD 0.10, TPU/GO-HMD 0.10, and TPU/GO-NH_3 0.10 nanocomposites are shown in Fig. 9. The TEM morphology of Fig. 9a and 9d, i.e., 0.1 wt% GO, and GO-NH_3 filled nanocomposites respectively are of

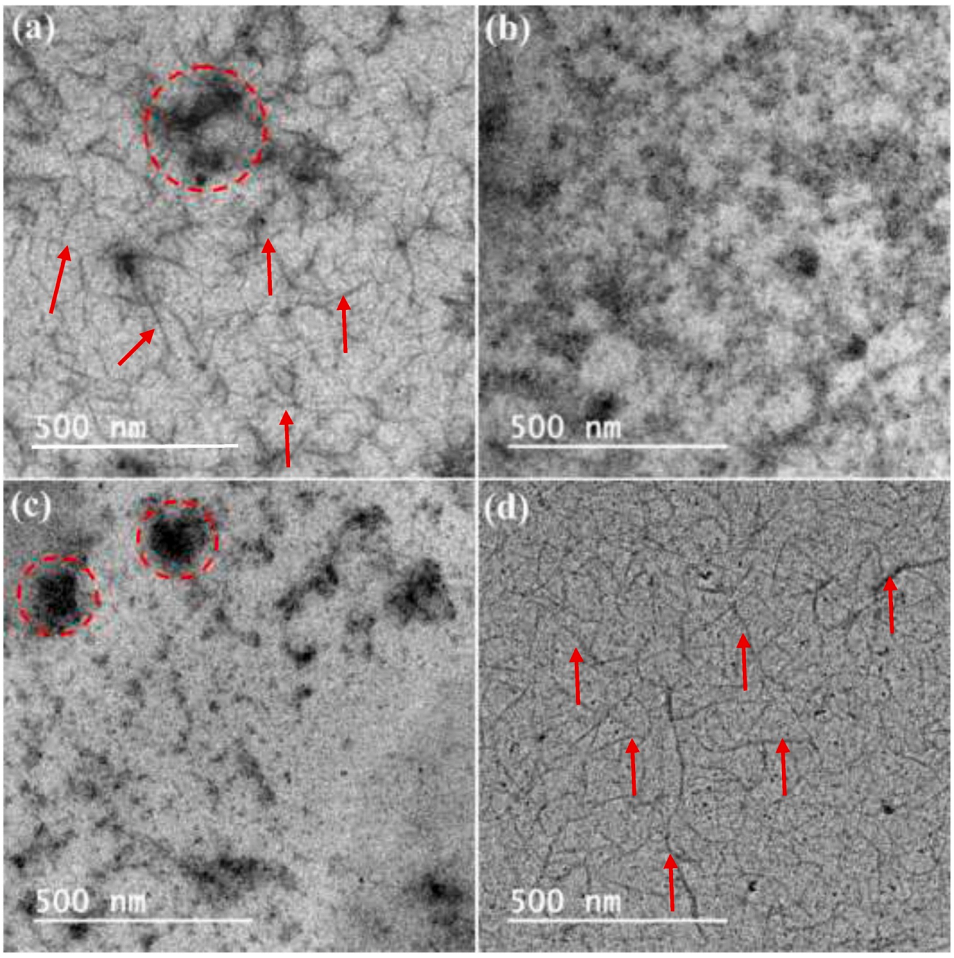

Fig. 9. Bright field TEM images of (a) TPU/GO 0.10 (b) TPU/GO-PPD 0.10 (c) TPU/GO-HMD 0.10 and (d) TPU/GO-NH_3 0.10.

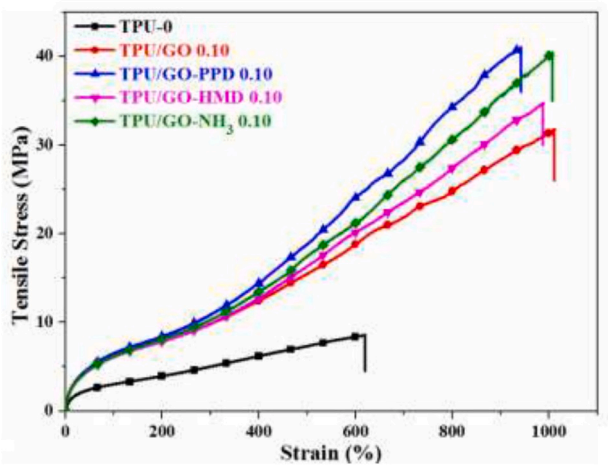

Fig. 10. Stress-strain curves of TPU/amine functionalized GO nanocomposites.

similar type. In these Figures, the lines represent the folded and crumpled GO or GO-NH_3 nanosheets, which are dispersed in the TPU matrix [44,45]. The folding arises due to a very larger size of GO/GO-NH_3, which was observed from their corresponding TEM image (Fig. 6). Also, strong π−π interaction among the nanosheets are also responsible for this [44]. The dark region in Fig. 9a represents the aggregation of GO layers. Therefore, from the TEM images, we can conclude GO-NH_3 disperse better in the TPU matrix compared to GO. The micrographs of

Table 2
Mechanical properties of TPU/amine functionalized GO nanocomposites.

Sample	Tensile strength (MPa)	Young's modulus (MPa)	Elongation at break (%)	Toughness (MPa)
TPU-0	8.6 ± 0.5	2.2 ± 0.1	618 ± 15	32.0 ± 1.2
TPU/GO 0.10	31.7 ± 1.5	3.5 ± 0.1	1010 ± 35	166.7 ± 2.5
TPU/GO-PPD 0.10	41.1 ± 1.7	5.4 ± 0.2	942 ± 27	183.9 ± 5.2
TPU/GO-HMD 0.10	34.8 ± 1.4	3.8 ± 0.2	988 ± 25	170.0 ± 3.9
TPU/GO-NH_3 0.10	40.2 ± 1.8	4.9 ± 0.2	1002 ± 32	192.9 ± 4.7

Fig. 9b and 9c are quite similar types, and the only difference is the level of dispersion of the nanosheets. In the case of GO-PPD filled nanocomposite (Fig. 9b), the nanosheets are well distributed throughout the matrix. But, for GO-HMD filled nanocomposite, there is some aggregation in the TEM image (Fig. 9c), and the aggregation is quite higher than that of Fig. 9a. So, TEM microstructural characterization revels that Fig. 9c has the poorest nanofiller distribution among all. The observed results give an idea about the mechanical properties, which can be found in the following section. In our previous work, a similar type of TEM morphology was observed for GO, and GO-PPD filled polyurethane nanocomposites [44].

Wu et al. [18] and Raghu et al. [46] also reported a similar type of microstructure for waterborne polyurethane/functionalized graphene

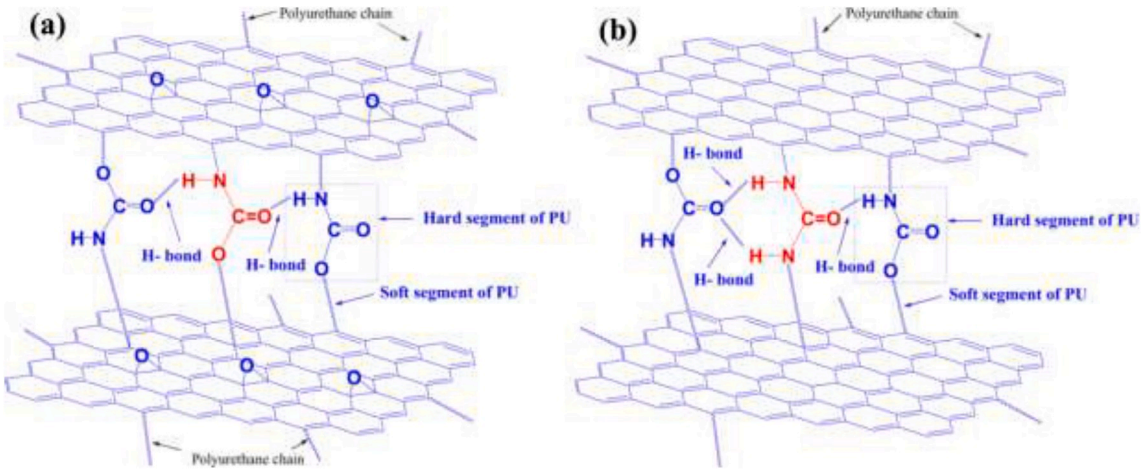

Fig. 11. (a) Monodentate H-bonding interaction between the urethane linkage of TPU grafted GO and the hard segment of adjacent TPU chain; (b) bidentate H-bonding interaction between the urea linkage of TPU grafted GOA and the hard segment of adjacent TPU chain.

nanocomposites.

4.5. Mechanical properties

4.5.1. Tensile properties

The incorporation of nanofiller to a polymer matrix results in an increase in mechanical properties. But, the nature of filler plays an important role in it. In this work, different types of amine functionalized GO has been added to the TPU matrix at a concentration of 0.10 wt%, and their effect in tensile properties have been observed. The typical stress-strain curve of TPU and its polymer nanocomposites has been presented in Fig. 10, and the corresponding value of tensile strength, Young's modulus and elongation at break have been summarized in Table 2. It is quite easy to understand that tensile strength, modulus, and elongation at break increases remarkably after adding 0.10 wt% of GO, GO-PPD, GO-HMD or GO-NH_3 to TPU. There are various reasons behind such remarkable improvement in tensile strength. The main reason is the strain hardening facilitated by the presence of graphene-based filler [9]. Orientation of the TPU grafted nanosheets and the soft segments of TPU along the tensile direction also contribute to a great extent in the enhancement of tensile strength [7]. Covalent bond formation between the NCO-terminated polyurethane pre-polymer and the GO or amine functionalized GO is also responsible for such improvement in mechanical properties [9,39]. The reasons behind the improvement of Young's modulus are covalent bonding, H-bonding and/or other polar-polar interactions between the hard segment of TPU and the urea linkage of amine functionalized GO/TPU nanocomposites which makes the hard domain stiff [47]. Interestingly, all the amine functionalized GO-based TPU nanocomposites possess superior mechanical properties compared to unmodified GO-based nanocomposite at ultra-low loading (0.10 wt%). There are a number of reasons behind such observation. (i) From the FESEM analysis (Fig. 8), it is clear that the dispersion of graphene-based fillers in the TPU matrix follows the order GO-PPD > GO-NH_3>GO-HMD > GO. Further, from TEM analysis (Fig. 9), it is observed that the dispersion of GO-PPD and GO-NH_3 is better than GO and GO-HMD. (ii) Amine functionalized GOs itself have superior mechanical properties compared to GO [48]. So, amine functionalized GO-based TPU nanocomposites must have better mechanical properties than GO-based nanocomposites. (iii) The strength and stability of urea linkage, formed during the preparation of amine functionalized GO (GOA)/TPU nanocomposites is higher than urethane linkage formed during the preparation of TPU/GO nanocomposite. Further, urea linkage of TPU grafted amine functionalized GO can form bidentate H- bonding interaction with the hard segment of adjacent TPU chain. Whereas, urethane linkage of TPU grafted GO can form only monodentate H-bonding interaction with the hard segment of adjacent TPU chain (Fig. 11), making the system stiffer. Hence, the mechanical properties of all amine functionalized GO/TPU nanocomposites are higher than TPU/GO nanocomposite. From XPS analysis, it is clear that nitrogen content in GO-PPD, GO-NH_3, and GO-HMD is 10.13%, 7.58%, and 4.17%, respectively (Table 1). Higher nitrogen content in amine functionalized GO implies the higher amount of amine modifier in amine functionalized GO and hence higher number of bidentate H-bonding interaction, which increases the tensile strength of the nanocomposite. Thus considering all the factors, it can be concluded that improvement in the tensile strength of TPU nanocomposites follows the order of GO-PPD > GO-NH_3>GO-HMD > GO, and the explanation matches with the experimental results. The quantities of amine functionalized GO added the same in all cases. Still, the amine modifier was different, and hence they influenced the mechanical properties of TPU to a different extent. The results show that PPD functionalized GO (GO-PPD) has the maximum influence in enhancing tensile strength and Young's modulus. Tensile strength of TPU increases by 378%, and Young's modulus increases by 146% after adding just 0.10 wt% GO-PPD. Elongation at break is maximum for 0.10 wt% GO filled nanocomposites (1010%). In other cases, also, the value is quite high, and the average enhancement in elongation at break is ~ 60%. This is due to the fact that at very low loading graphene-based materials act a plasticizer by occupying a position between the TPU chains and thus increases free volume [49] and elongation at break. Rupturing of H-bond between the TPU grafted graphene-based materials and the adjacent TPU chain and slipping of nanosheets during tensile loading is also responsible for the enhancement of elongation at break [9].

Toughness is the amount of energy absorbed per unit volume of a sample before getting a failure. It is calculated from the total area under the stress-strain curve. A material having high strength as well as high ductility will have high toughness. TPU/GO-PPD 0.10 has higher tensile strength than TPU/GO-NH_3 0.10, but elongation at break is higher for TPU/GO-NH_3 0.10 resulting maximum toughness of 192.9 MPa for TPU/GO-NH_3 0.10.

4.5.2. Cyclic loading-unloading behavior

Resilience is one of the most important mechanical properties of a thermoplastic elastomer. To investigate the resilience of TPU and its nanocomposites; cyclic tensile loading-unloading experiments were performed at a constant speed of 100 mm/min and up to 10 cycles for each sample, and the results are presented in Fig. 12.

It was observed that all nanocomposite samples recover to a greater extent compared to pristine TPU after stretching 200%. It was also noticed that the percent recovery for TPU nanocomposites with amine

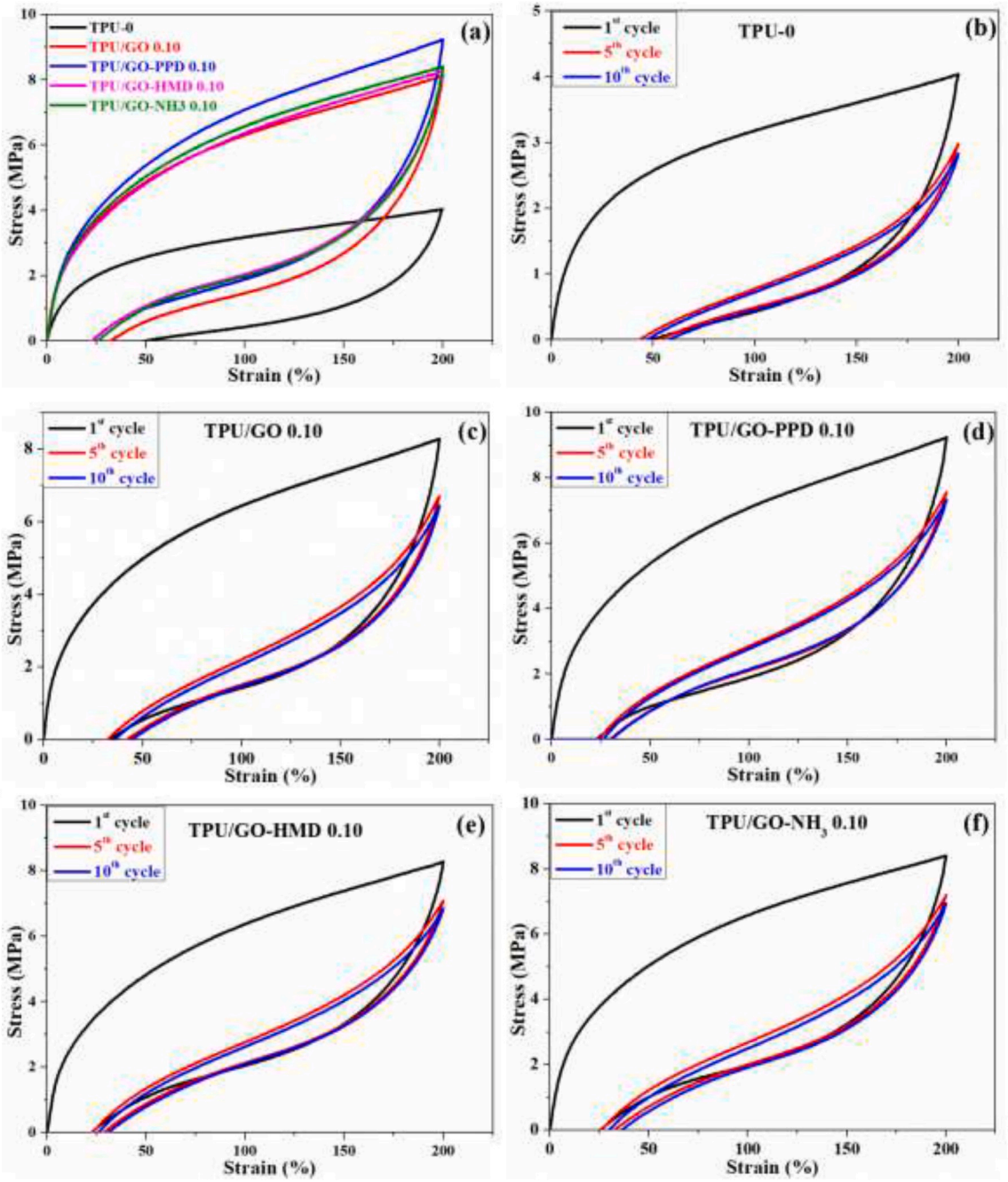

Fig. 12. (a) First cycle of loading-unloading curve for TPU and its nanocomposites with 0.10 wt % filler; First, fifth and tenth cycles of loading-unloading curve for (b) TPU 0, (c) TPU/GO 0.10, (d) TPU/GO-PPD 0.10, (e) TPU/GO-HMD 0.10 and (f) TPU/GO-NH_3 0.10.

functionalized GO is higher compared to TPU/GO nanocomposites. These results clearly indicate that the resilience of TPU was enhanced with the incorporation of 0.10 wt% GO and amine functionalized GO, and the improvement was more prominent in the case of amine functionalized GO. The possible reason behind such observation is the formations of more stable urea linkages by the amine functionalized GO during the in-situ synthesis of polyurethane nanocomposites [18]. Further, the amount of stress required for loading-unloading was enhanced with the addition of 0.10 wt% nanomaterials, and it was maximum in the case of TPU/GO-PPD 0.10. The results were in agreement with tensile data. The comparative effects of 1st, 5th, and 10th cycles at 200% elongation for TPU/GO 0.10, TPU/GO-PPD 0.10, TPU/GO-HMD 0.10 and TPU/GO-NH_3 0.10 are presented in Fig. 12c-f, respectively. It was found that the amount of stress required for 200% elongation decreases with an increase in a number of the number of cycles (Fig. 13a), and the resilience values also follow the same trend (Fig. 13b). This is due to the fatigue behavior of the material, which causes the molecular chain scission and hence weakens the material. Bai et al. [50] reported a similar type of results for polyhedral oligomeric silsesquioxane (POSS) crosslinked poly(styrene-b-butadiene-b-styrene) elastomer and found that POSS improves the mechanical properties of SEBS elastomer including resilience. Zhang et al. [51] also investigated the cyclic tensile loading-unloading behavior of poly (vinyl alcohol) hydrogels and found similar type results.

4.6. Thermogravimetric analysis (TGA)

The thermal degradation behavior of TPU and its nanocomposites in

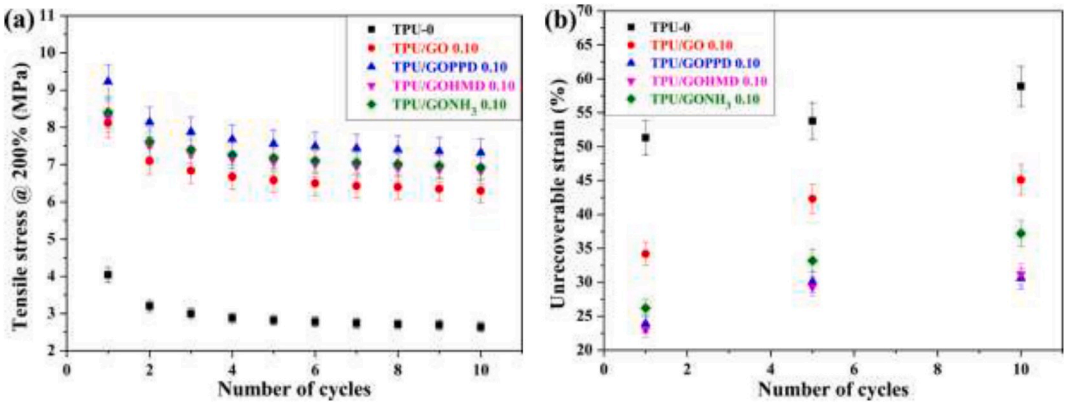

Fig. 13. (a) Variation of tensile stress at 200% elongation with a number of cycles; (b) change of unrecoverable strain (%) with the number of loading-unloading cycles.

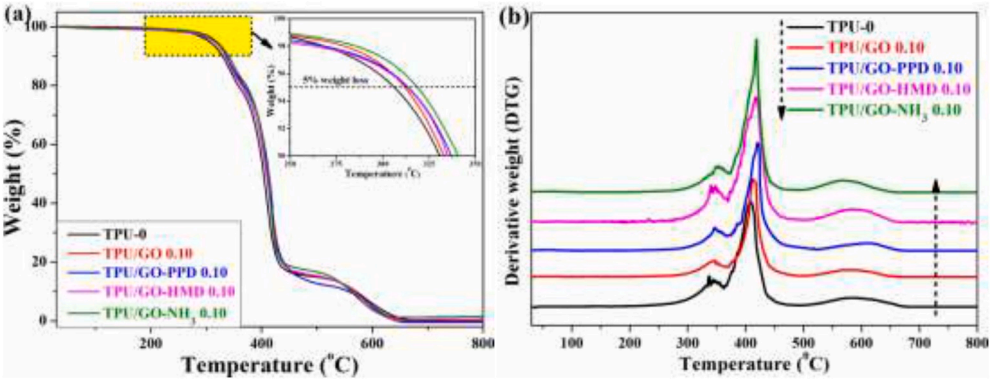

Fig. 14. (a) TGA and (b) DTG thermograms of TPU/amine functionalized GO nanocomposites.

Table 3
TGA results of TPU/amine functionalized GO nanocomposites.

Sample	T_{in} (°C)	T_{max} (°C)
TPU-0	306.2	407.5
TPU/GO 0.10	312.0	414.0
TPU/GO-PPD 0.10	313.5	421.0
TPU/GO-HMD 0.10	313.0	418.0
TPU/GO-NH_3 0.10	318.6	419.0

Table 4
DMTA results of TPU/amine functionalized GO nanocomposites.

Samples	$T_{g,s}$ (°C)	Log E′ at −25 °C (MPa)	Log E′ at 0 °C (MPa)	Log E′ at 25 °C (MPa)
TPU-0	−59.5	2.14	1.90	1.34
TPU/GO 0.10	−65.5	2.30	1.95	1.42
TPU/GO-PPD 0.10	−67.8	2.40	2.07	1.53
TPU/GO-HMD 0.10	−71.0	2.32	1.98	1.46
TPU/GO-NH_3 0.10	−70.2	2.35	2.03	1.48

the nitrogen atmosphere were investigated by TGA. TGA and the corresponding differential thermograms (DTG) of TPU and its nanocomposites are presented in Fig. 14. From the TGA thermograms (Fig. 14a) it is clear that both TPU and its nanocomposites show two-stage degradation behavior where the first stage corresponds to the degradation of the soft segment, and the second stage corresponds to the degradation of the hard segment [5,39,47]. Temperature for 5% weight loss was considered as initial degradation temperature (T_{in}). Temperatures such as maximum rate of degradation (T_{max}) and T_{in} for TPU and nanocomposites are summarized in Table 3. From Table 4 it is clear that both the T_{in} and T_{max} increases significantly after incorporating 0.10 wt % nanofiller, and the increment is more prominent in the case of amine functionalized GO-based nanocomposites compared to TPU/GO. Amine functionalization has a positive influence in enhancing the thermal stability of TPU nanocomposites. Again, TPU/GO-PPD 0.10 shows maximum increments in thermal stability compared to other amine functionalized GO-based TPU nanocomposites. With the incorporation of just 0.10 wt% GO-PPD, T_{in} increases by 7°C and T_{max} increases by 13.5°C. This is due to higher thermal stability of GO-PPD compared to other graphene based materials. Enhanced thermal stability of nanocomposites compared to pristine TPU was due to different kinds of physical and chemical interactions between TPU and the graphene based nanofillers [47]. The observed results are in line with that reported by Wu et al. [18] and Zhang et al. [52] for TPU and functionalized graphene system.

4.7. Dynamic mechanical thermal analysis (DMTA)

DMTA was carried out to scrutinize the influence of reinforcing fillers in the mechanical properties of polyurethane over a broad range of temperature. Fig. 15a shows the variation of storage modulus ($E^{'}$) with temperature and Fig. 15b shows the variation of the damping factor (tanδ) with temperature. As seen in Fig. 15a, $E^{'}$ value of TPU increases with the incorporation of 0.10 wt% filler. This is due to various physicochemical interactions between TPU and graphene-based filler [9]. Further, all the amine functionalized GO filled nanocomposites exhibit better improvement in storage modulus compared to unmodified GO

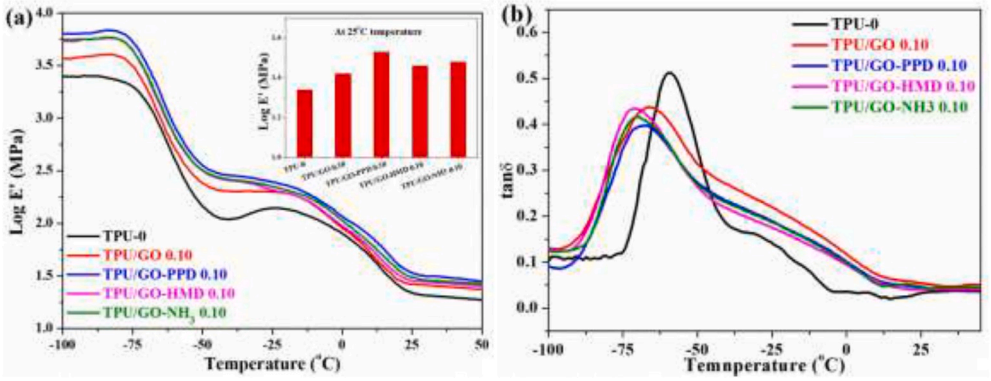

Fig. 15. DMTA curves of TPU/amine functionalized GO nanocomposites: (a) Storage modulus, (b) tan δ

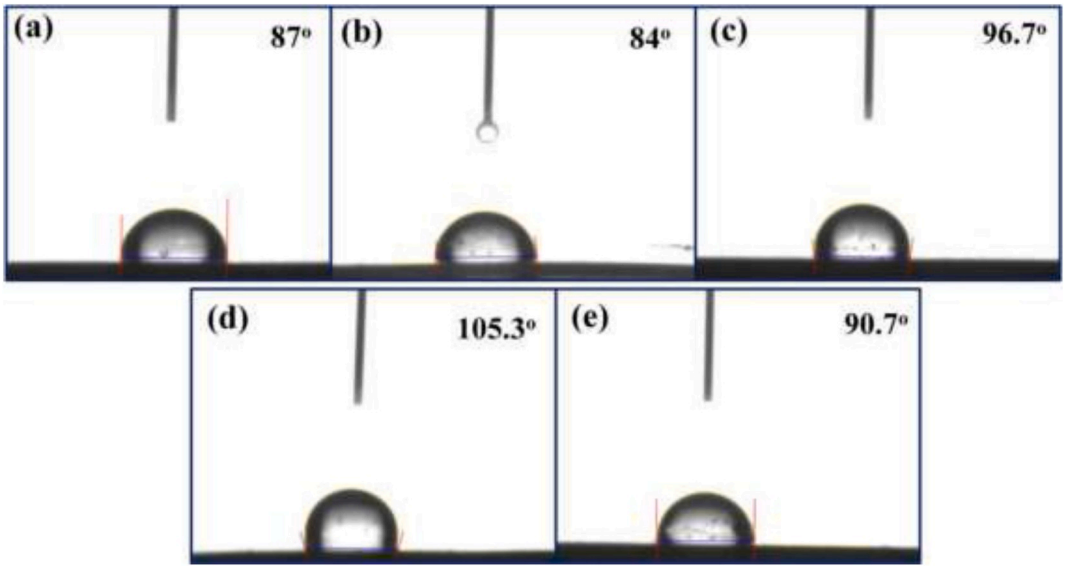

Fig. 16. Water contact angle of (a) TPU-0, (b) TPU/GO 0.10, (c) TPU/GO-PPD 0.10, (d) TPU/GO-HMD 0.10 and (e) TPU/GO-NH_3 0.10.

Table 5
Surface properties of TPU/amine functionalized GO nanocomposites by contact angle analysis.

Sample	Contact angle (°)	Surface energy (mJm^{-2})	Work of adhesion (mN m^{-1})
TPU-0	87.0 ± 1.4	20.2 ± 1.0	76.6 ± 1.7
TPU/GO 0.10	84.0 ± 1.2	22.2 ± 0.8	80.4 ± 1.5
TPU/GO-PPD 0.10	96.7 ± 1.6	14.2 ± 0.9	64.3 ± 2.0
TPU/GO-HMD 0.10	105.3 ± 2.3	9.8 ± 0.9	53.6 ± 2.8
TPU/GO-NH_3 0.10	90.7 ± 1.9	17.7 ± 1.1	71.9 ± 2.4

filled composites signifying a positive influence of amine functionalization in the mechanical properties of TPU [18]. The effect becomes most significant for PPD functionalized GO filled composite at similar loading. Table 4 shows that storage modulus increases with a decrease in temperature. This is due to the restriction in the movement of the polymer chain at a lower temperature. The variation of storage modulus at 25°C for TPU and its nanocomposites is shown in the inset of Fig. 15a. Glass transition temperature of soft segment ($T_{g,s}$) is derived from the maximum position of tanδ vs. temperature plot. Fig. 15b shows that $T_{g,s}$ decreases with the addition of GO and amine functionalized GO. This is due to increase in micro phase separation between hard and soft segment [14].

4.8. Contact angle analysis

Contact angle measurement is one of the easiest ways to determine the wettability of a solid surface. The contact angle of a material is very important for its various applications like biomedical, paints, packaging, etc. [53]. The contact angle can be measured by using a number of liquids like water, ethylene glycol, glycerol, etc. [54]. In this study, water (surface tension = 72.8 mJ m^{-2}) was taken as a testing liquid, and all measurements were done by a sessile drop method. The water contact angle of TPU and its nanocomposite films are shown in Fig. 16 and the corresponding value of surface energy and work of adhesion are presented in Table 5.

The water contact angle on TPU film was 87°, which is comparable to earlier reported data [55]. With the incorporation of GO (contact angle = 57°), the water contact angle value decreases from 87° to 84°. This is due to the hydrophilic nature of the wrinkled GO sheets [56]. In the case of amine functionalized GO-based nanocomposites, the contact angle increases with the addition of 0.10 wt% nanosheets.

The amount of increment was different for different amine-modified GO depending upon the nature of amine-modified GO. It was clear that the contact angle and C/O ratio of GO-HMD was maximum among all amine-modified GOs. Hence, TPU/GO-HMD 0.10 shows the maximum improvement in contact angle value. From Table 5, it can be concluded

that amine functionalization helps to increase the contact angle of TPU, making the film hydrophobic. Surface energy and work of adhesion are the two most fundamental surface properties of a material. These two properties cannot be measured directly. They can be calculated by utilizing the contact angle result and using empirical models.

Surface energy can be calculated by several empirical models [57]. Among them, Girifalco-Good-Fowkes-Young (GGFY) model is mainly used for one liquid and one solid system. The surface energy of TPU and its composites surface were calculated by using GGFY equation (Eq. (1))

$$\gamma_{SV} = \frac{1}{4(1 + Cos\theta)^2 \gamma_{LV}} \quad (1)$$

Here, γ_{SV} is the surface energy of the solid surface, γ_{LV} is the surface energy between pure water and air (72.8 mJ m^{-2}) and θ is the contact angle.

The work of adhesion was calculated by using the Young–Dupré equation [58] as shown in Eq. (2).

$$W_a = \gamma_{LV}(1 + \mathrm{Cos}\theta) \quad (2)$$

From Table 5 it is seen that surface energy and work of adhesion decreases with an increase in water contact angle vice versa. Deshmukh et al. [54] reported the variation of contact angle, work of adhesion, and surface energy of polyvinyl chloride (PVC) with GO addition.

5. Conclusions

In the present work, p-phenylenediamine (PPD), hexamethylene diamine (HMD), and liquid NH_3 functionalized GO were synthesized by chemical reaction of the amine modifiers individually with GO dispersion. Reduction of GO occurs simultaneously during functionalization proved by FTIR, Raman spectroscopy, UV–Visible spectroscopy, XPS and XRD. The prepared amine functionalized GOs were used for the fabrication of polyurethane nanocomposites by the in-situ solution polymerization technique. Nano filler loading in nanocomposite was restricted to just 0.1 wt% for the current study and the influence of *p*-phenylenediamine (PPD), hexamethylene diamine (HMD) and liquid NH_3 functionalized GO in the thermal, mechanical and surface properties of TPU was investigated. From the experimental results, it is clear that amine functionalization has a positive influence on thermal, mechanical, and other properties. Among all amine functionalized GOs, GO-PPD shows a more significant impact in enhancing the thermal and mechanical properties. With the incorporation of just 0.1 wt% GO-PPD, tensile strength improves by 378%, and Young's modulus increases by 145%. In addition to this thermal stability of the polyurethane also increases by 13 °C with only 0.1 wt% loading of GO-PPD. Resilience property of the polyurethane as observed from the cyclic tensile loading-unloading curve shows that incorporation of GO or amine functionalized GO improves it, and the improvement becomes more prominent in the case of amine functionalized GO. Contact angle analysis data reveals that the nanocomposite surface becoming hydrophobic for amine functionalized GO filled nanocomposites and the hydrophobicity is maximum in case of HMD functionalized GO filled TPU nanocomposites (water contact angle = 105°). The improved mechanical, thermal properties, and hydrophobicity of the composite materials can have potential application opportunities in flexible pipes, airplane interior parts, hydrophobic coatings, automobile interior parts, etc.

Declaration of competing interest

The authors declare no conflict of interest.

CRediT authorship contribution statement

Madhab Bera: Supervision. **Arjun Prabhakar:** Formal analysis. **Pradip K. Maji:** Supervision.

Appendix A. Supplementary data

Supplementary data to this article can be found online at https://doi.org/10.1016/j.compositesb.2020.108075.

References

[1] Hepburn C. Polyurethane elastomers. Springer Netherlands; 1992.
[2] Maji PK, Guchhait PK, Bhowmick AK. Effect of nanoclays on physico-mechanical properties and adhesion of polyester-based polyurethane nanocomposites: structure–property correlations. J Mater Sci 2009;44:5861–71. https://doi.org/10.1007/s10853-009-3827-7.
[3] Dong M, Li Q, Liu H, Liu C, Wujcik EK, Shao Q, Ding T, Mai X, Shen C, Guo Z. Thermoplastic polyurethane-carbon black nanocomposite coating: fabrication and solid particle erosion resistance. Polymer 2018;158:381–90. https://doi.org/10.1016/J.POLYMER.2018.11.003.
[4] Wang Y, Cheng Z, Liu Z, Kang H, Liu Y. Cellulose nanofibers/polyurethane shape memory composites with fast water-responsivity. J Mater Chem B 2018;6:1668–77. https://doi.org/10.1039/C7TB03069J.
[5] Askari F, Barikani M, Barmar M, Shokrollahi P. Polyurethane/amino-grafted multiwalled carbon nanotube nanocomposites: microstructure, thermal, mechanical, and rheological properties. J Appl Polym Sci 2017;134. https://doi.org/10.1002/app.44411.
[6] Liao K-H, Qian Y, Macosko CW. Ultralow percolation graphene/polyurethane acrylate nanocomposites. Polymer 2012;53:3756–61. https://doi.org/10.1016/J.POLYMER.2012.06.020.
[7] Chen Z, Lu H. Constructing sacrificial bonds and hidden lengths for ductile graphene/polyurethane elastomers with improved strength and toughness. J Mater Chem 2012;22:12479. https://doi.org/10.1039/c2jm30517h.
[8] Lee YR, Raghu AV, Jeong HM, Kim BK. Properties of waterborne polyurethane/functionalized graphene sheet nanocomposites prepared by an in situ method. Macromol Chem Phys 2009;210:1247–54. https://doi.org/10.1002/macp.200900157.
[9] Pokharel P, Choi S, Lee DS. The effect of hard segment length on the thermal and mechanical properties of polyurethane/graphene oxide nanocomposites. Composer Part A Appl Sci Manuf 2015;69:168–77. https://doi.org/10.1016/J.COMPOSITESA.2014.11.010.
[10] Thakur S, Karak N. Multi-stimuli responsive smart elastomeric hyperbranched polyurethane/reduced graphene oxide nanocomposites. J Mater Chem A 2014;2:14867–75. https://doi.org/10.1039/C4TA02497D.
[11] Zhu Y, Murali S, Cai W, Li X, Suk JW, Potts JR, Ruoff RS. Graphene and graphene oxide: synthesis, properties, and applications. Adv Mater 2010;22:3906–24. https://doi.org/10.1002/adma.201001068.
[12] Morozov SV, Novoselov KS, Katsnelson MI, Schedin F, Elias DC, Jaszczak JA, Geim AK. Giant intrinsic carrier mobilities in graphene and its bilayer. Phys Rev Lett 2008;100:016602. https://doi.org/10.1103/PhysRevLett.100.016602.
[13] Hou W, Tang B, Lu L, Sun J, Wang J, Qin C, Dai L. Preparation and physico-mechanical properties of amine-functionalized graphene/polyamide 6 nanocomposite fiber as a high performance material. RSC Adv 2014;4:4848. https://doi.org/10.1039/c3ra46525j.
[14] Pokharel P, Lee SH, Lee DS. Thermal, mechanical, and electrical properties of graphene nanoplatelet/graphene oxide/polyurethane hybrid nanocomposite. J Nanosci Nanotechnol 2015;15:211–4. https://doi.org/10.1166/jnn.2015.8353.
[15] Ma W, Wu L, Zhang D, Wang S. Preparation and properties of 3-aminopropyltriethoxysilane functionalized graphene/polyurethane nanocomposite coatings. Colloid Polym Sci 2013;291:2765–73. https://doi.org/10.1007/s00396-013-3014-x.
[16] Yang L, Phua SL, Toh CL, Zhang L, Ling H, Chang M, Zhou D, Dong Y, Lu X. Polydopamine-coated graphene as multifunctional nanofillers in polyurethane. RSC Adv 2013;3:6377. https://doi.org/10.1039/c3ra23307c.
[17] Bandyopadhyay P, Park WB, Layek RK, Uddin ME, Kim NH, Kim H-G, Lee JH. Hexylamine functionalized reduced graphene oxide/polyurethane nanocomposite-coated nylon for enhanced hydrogen gas barrier film. J Membr Sci 2016;500:106–14. https://doi.org/10.1016/J.MEMSCI.2015.11.029.
[18] Wu S, Shi T, Zhang L. Preparation and properties of amine-functionalized reduced graphene oxide/waterborne polyurethane nanocomposites. High Perform Polym 2016;28:453–65. https://doi.org/10.1177/0954008315587124.
[19] Sadasivuni KK, Ponnamma D, Kumar B, Strankowski M, Cardinaels R, Moldenaers P, Thomas S, Grohens Y. Dielectric properties of modified graphene oxide filled polyurethane nanocomposites and its correlation with rheology. Compos Sci Technol 2014;104:18–25. https://doi.org/10.1016/J.COMPSCITECH.2014.08.025.
[20] Ramezanzadeh B, Ghasemi E, Mahdavian M, Changizi E, Mohamadzadeh Moghadam MH. Characterization of covalently-grafted polyisocyanate chains onto graphene oxide for polyurethane composites with improved mechanical properties. Chem Eng J 2015;281:869–83. https://doi.org/10.1016/J.CEJ.2015.07.027.
[21] Bera M, Maji PK. Effect of structural disparity of graphene-based materials on thermo-mechanical and surface properties of thermoplastic polyurethane nanocomposites. Polymer 2017;119:118–33. https://doi.org/10.1016/J.POLYMER.2017.05.019.
[22] Bera M, Chandravati, Gupta P, Maji PK. Facile one-pot synthesis of graphene oxide by sonication assisted mechanochemical approach and its surface chemistry. J Nanosci Nanotechnol 2018;18:902–12. https://doi.org/10.1166/jnn.2018.14306.

[23] Ma H-L, Zhang H-B, Hu Q-H, Li W-J, Jiang Z-G, Yu Z-Z, Dasari A. Functionalization and reduction of graphene oxide with *p* -phenylene diamine for electrically conductive and thermally stable polystyrene composites. ACS Appl Mater Interfaces 2012;4:1948–53. https://doi.org/10.1021/am201654b.
[24] Wu Y, Lin X, Shen X, Sun X, Liu X, Wang Z, Kim J-K. Exceptional dielectric properties of chlorine-doped graphene oxide/poly (vinylidene fluoride) nanocomposites. Carbon N. Y. 2015;89:102–12. https://doi.org/10.1016/J.CARBON.2015.02.074.
[25] Ryu SH, Sin JH, Shanmugharaj AM. Study on the effect of hexamethylene diamine functionalized graphene oxide on the curing kinetics of epoxy nanocomposites. Eur Polym J 2014;52:88–97. https://doi.org/10.1016/J.EURPOLYMJ.2013.12.014.
[26] Verma S, Dutta RK. A facile method of synthesizing ammonia modified graphene oxide for efficient removal of uranyl ions from aqueous medium. RSC Adv 2015;5:77192–203. https://doi.org/10.1039/C5RA10555B.
[27] Marcano DC, Kosynkin DV, Berlin JM, Sinitskii A, Sun Z, Slesarev A, Alemany LB, Lu W, Tour JM. Improved synthesis of graphene oxide. ACS Nano 2010;4:4806–14. https://doi.org/10.1021/nn1006368.
[28] Kumar NA, Gambarelli S, Duclairoir F, Bidan G, Dubois L. Synthesis of high quality reduced graphene oxide nanosheets free of paramagnetic metallic impurities. J Mater Chem A 2013;1:2789–94. https://doi.org/10.1039/C2TA01036D.
[29] Huang H, Xia Y, Tao X, Du J, Fang J, Gan Y, Zhang W. Highly efficient electrolytic exfoliation of graphite into graphene sheets based on Li ions intercalation–expansion–microexplosion mechanism. J Mater Chem 2012;22:10452. https://doi.org/10.1039/c2jm00092j.
[30] Ryu SH, Sin JH, Shanmugharaj AM. Study on the effect of hexamethylene diamine functionalized graphene oxide on the curing kinetics of epoxy nanocomposites. Eur Polym J 2014;52:88–97. https://doi.org/10.1016/J.EURPOLYMJ.2013.12.014.
[31] Verma S, Dutta RK. A facile method of synthesizing ammonia modified graphene oxide for efficient removal of uranyl ions from aqueous medium. RSC Adv 2015;5:77192–203. https://doi.org/10.1039/C5RA10555B.
[32] Kotal M, Banerjee SS, Bhowmick AK. Functionalized graphene with polymer as unique strategy in tailoring the properties of bromobutyl rubber nanocomposites. Polymer 2016;82:121–32. https://doi.org/10.1016/J.POLYMER.2015.11.044.
[33] Liu H, Kuila T, Kim NH, Ku BC, Lee JH. In situ synthesis of the reduced graphene oxide–polyethyleneimine composite and its gas barrier properties. J Mater Chem 2013;1:3739–46. https://doi.org/10.1039/C3TA01228J.
[34] Caliman CC, Mesquita AF, Cipriano DF, Freitas JCC, Cotta AAC, Macedo WAA, Porto AO. One-pot synthesis of amine-functionalized graphene oxide by microwave-assisted reactions: an outstanding alternative for supporting materials in supercapacitors. RSC Adv 2018;8:6136–45. https://doi.org/10.1039/C7RA13514A.
[35] Yuan B, Bao C, Song L, Hong N, Liew KM, Hu Y. Preparation of functionalized graphene oxide/polypropylene nanocomposite with significantly improved thermal stability and studies on the crystallization behavior and mechanical properties. Chem Eng J 2014;237:411–20. https://doi.org/10.1016/J.CEJ.2013.10.030.
[36] Stobinski L, Lesiak B, Malolepszy A, Mazurkiewicz M, Mierzwa B, Zemek J, Jiricek P, Bieloshapka I. Graphene oxide and reduced graphene oxide studied by the XRD, TEM and electron spectroscopy methods. J Electron Spectrosc Relat Phenom 2014;195:145–54. https://doi.org/10.1016/J.ELSPEC.2014.07.003.
[37] Tang L-C, Wan Y-J, Yan D, Pei Y-B, Zhao L, Li Y-B, Wu L-B, Jiang J-X, Lai G-Q. The effect of graphene dispersion on the mechanical properties of graphene/epoxy composites. Carbon N. Y. 2013;60:16–27. https://doi.org/10.1016/J.CARBON.2013.03.050.
[38] Yılgör E, Yılgör İ, Yurtsever E. Hydrogen bonding and polyurethane morphology. I. Quantum mechanical calculations of hydrogen bond energies and vibrational spectroscopy of model compounds. Polymer 2002;43:6551–9. https://doi.org/10.1016/S0032-3861(02)00567-0.
[39] Thakur S, Karak N. Ultratough, ductile, Castor oil-based, hyperbranched, polyurethane nanocomposite using functionalized reduced graphene oxide. ACS Sustain Chem Eng 2014;2:1195–202. https://doi.org/10.1021/sc500165d.
[40] Kaur G, Adhikari R, Cass P, Bown M, Evans MDM, Vashi AV, Gunatillake P. Graphene/polyurethane composites: fabrication and evaluation of electrical conductivity, mechanical properties and cell viability. RSC Adv 2015;5:98762–72. https://doi.org/10.1039/C5RA20214K.
[41] Wu S, Shi T, Zhang L. Preparation and properties of amine-functionalized reduced graphene oxide/waterborne polyurethane nanocomposites. High Perform Polym 2016;28:453–65. https://doi.org/10.1177/0954008315587124.
[42] Pokharel P, Lee DS. High performance polyurethane nanocomposite films prepared from a masterbatch of graphene oxide in polyether polyol. Chem Eng J 2014;253:356–65. https://doi.org/10.1016/J.CEJ.2014.05.046.
[43] Wu Y, Lin X, Shen X, Sun X, Liu X, Wang Z, Kim J-K. Exceptional dielectric properties of chlorine-doped graphene oxide/poly (vinylidene fluoride) nanocomposites. Carbon N. Y. 2015;89:102–12. https://doi.org/10.1016/J.CARBON.2015.02.074.
[44] Bera M, Gupta P, Maji PK. Efficacy of ultra-low loading of amine functionalized graphene oxide into glycidol-terminated polyurethane for high-performance composite material. React Funct Polym 2019;139:60–74. https://doi.org/10.1016/J.REACTFUNCTPOLYM.2019.03.008.
[45] Strankowski M, Korzeniewski P, Strankowska J, AS A, Thomas S, Strankowski M, Korzeniewski P, Strankowska J, AS A, Thomas S. Morphology, mechanical and thermal properties of thermoplastic polyurethane containing reduced graphene oxide and graphene nanoplatelets. Materials 2018;11:82. https://doi.org/10.3390/ma11010082.
[46] Raghu AV, Lee YR, Jeong HM, Shin CM. Preparation and physical properties of waterborne polyurethane/functionalized graphene sheet nanocomposites. Macromol Chem Phys 2008;209:2487–93. https://doi.org/10.1002/macp.200800395.
[47] Thakur S, Karak N. A tough, smart elastomeric bio-based hyperbranched polyurethane nanocomposite. New J Chem 2015;39:2146–54. https://doi.org/10.1039/C4NJ01989J.
[48] Wang H, Liu X, Yang Z, He H, Shao X, Bai R. Preparation and characterization of hexamethylenediamine-modified graphene oxide/Co-polyamide nanocomposites. Polym Polym Compos 2019:1–12. https://doi.org/10.1177/0967391119887298.
[49] Kaveh P, Mortezaei M, Barikani M, Khanbabaei G. Low-temperature flexible polyurethane/graphene oxide nanocomposites: effect of polyols and graphene oxide on physicomechanical properties and gas permeability. Polym Plast Technol Eng 2014;53:278–89. https://doi.org/10.1080/03602559.2013.844241.
[50] Bai J, Shi Z, Yin J, Tian M. A simple approach to preparation of polyhedral oligomeric silsesquioxane crosslinked poly(styrene-b-butadiene-b-styrene) elastomers with a unique micro-morphology via UV-induced thiol–ene reaction. Polym Chem 2014;5:6761–9. https://doi.org/10.1039/C4PY00780H.
[51] Zhang J, Cao Y, Feng J, Wu P. Graphene-oxide-sheet-Induced gelation of cellulose and promoted mechanical properties of composite aerogels. J Phys Chem C 2012;116:8063–8. https://doi.org/10.1021/jp2109237.
[52] Zhang J, Zhang C, Madbouly SA. *In situ* polymerization of bio-based thermosetting polyurethane/graphene oxide nanocomposites. J Appl Polym Sci 2015;132. https://doi.org/10.1002/app.41751.
[53] Feng L, Zhang X, Dai J, Ge Z, Chao J, Bai C. Synthesis and surface properties of polyurethane modified by polysiloxane. Front Chem China 2008;3:1–5. https://doi.org/10.1007/s11458-008-0001-8.
[54] Deshmukh K, Khatake SM, Joshi GM. Surface properties of graphene oxide reinforced polyvinyl chloride nanocomposites. J Polym Res 2013;20:286. https://doi.org/10.1007/s10965-013-0286-2.
[55] Paul D, Paul S, Roohpour N, Wilks M, Vadgama P, Paul D, Paul S, Roohpour N, Wilks M, Vadgama P. Antimicrobial, mechanical and thermal studies of silver particle-loaded polyurethane. J Funct Biomater 2013;4:358–75. https://doi.org/10.3390/jfb4040358.
[56] Pant HR, Pokharel P, Joshi MK, Adhikari S, Kim HJ, Park CH, Kim CS. Processing and characterization of electrospun graphene oxide/polyurethane composite nanofibers for stent coating. Chem Eng J 2015;270:336–42. https://doi.org/10.1016/J.CEJ.2015.01.105.
[57] A.W. Adamson, A.P. Gast, J. Wiley, Physical chemistry of surfaces sixth edition, n. d.
[58] Mittal KL. W. And A. (6th : 2008 : U. Of M. International symposium on contact angle, contact angle, wettability and adhesion. VSP; 2009.